

# Comparison of Acousto-optic and Liquid Crystal Tunable Filters for Laser-Induced Breakdown Spectroscopy

DIMITRA N. STRATIS, KRISTINE L. ELAND, J. CHANCE CARTER, SAMUEL J. TOMLINSON, and S. MICHAEL ANGEL\*

*Department of Chemistry and Biochemistry, The University of South Carolina, Columbia, South Carolina 29208*

In this paper, we report the first time-resolved laser-induced plasma images acquired using a liquid crystal tunable filter (LCTF). We also compare the use of LCTFs and acousto-optic tunable filters (AOTFs) for time-resolved plasma imaging applications in terms of resolution, out-of-band rejection, and image quality. Application of tunable filter technologies to plasma imaging is unlike other spectroscopic imaging methods because of the intense and spectrally broad background generated by a laser-induced plasma. High quality images of the distribution of atomic emission within a laser-induced plasma can be achieved using both AOTFs and LCTFs. However, additional filters are needed for rejection of wavelengths outside the tuning ranges of the devices. Both devices exhibited superior resolution in the lower working range of the filters (~500 nm) with the LCTF exhibiting superior spectral resolution to the AOTF.

Index Headings: LIBS; Laser-induced plasmas; Laser ablation; Tunable filters; AOTF; LCTF; Imaging; Plasma imaging; Laser-induced breakdown spectroscopy.

## INTRODUCTION

Laser-induced breakdown spectroscopy (LIBS) is a rapid form of elemental analysis that has potential for remote or online applications. In LIBS, virtually any type of sample can be rapidly analyzed by measuring the emission of the excited atoms and/or ions that comprise a laser-induced plasma generated on the sample of interest. Several reviews of LIBS have been published recently,<sup>1-4</sup> as well as a number of new applications.<sup>5-16</sup> LIBS possesses a number of advantages over other forms of atomic spectroscopy, with particular benefits gained in spatial and depth resolved analyses,<sup>6,10</sup> remote sensing,<sup>9,11,12</sup> operation in hostile environments,<sup>13-15</sup> and field-based applications.<sup>16</sup>

Although it is relatively simple to perform a LIBS analysis, the processes involved in laser-induced plasma formation (e.g., ablation, atomization, and excitation), are quite complex and difficult to reproduce.<sup>17</sup> In addition, LIBS analyses are complicated by a very intense background that exhibits large fluctuations. Consequently, the method suffers from poor detection limits and reproducibility compared to alternate forms of atomic spectroscopy. To address these problems and gain a better understanding of the factors that affect the LIBS signal, a great deal of research has been devoted to the characterization of laser-induced plasmas. Because of the significant changes in the intensity and spatial distribution of plasma emission, time-resolved plasma imaging is very useful for studying laser generated plasmas. In addition,

it is important to investigate the spatial distribution of the emission since the optimum region in the plasma in which to collect the LIBS signal varies for different elements,<sup>18-21</sup> and will change with different samples and matrices,<sup>22</sup> laser parameters,<sup>23-26</sup> and atmospheric conditions.<sup>27-30</sup> Many studies consider both the temporal and spatial development, but examine the spatial dependence simply by changing the field of view of the collection optics to a different region of the plasma. However, imaging the emission from a particular atomic line throughout the entire plasma offers many advantages over single-point measurements. Because imaging provides a means of monitoring the entire spatial distribution of the atomic emission from each laser-generated plasma, it provides a more rapid and more accurate analysis by being unaffected by the shot-to-shot variability of the plasma. Olesik et al. have compared a slitless spectrograph and a monochromatic imaging spectrometer for spatial mapping of inductively coupled plasmas and flames.<sup>31</sup> They showed that although the slitless spectrograph had poor spectral resolution, the imaging spectrometer provided both high spatial and spectral resolution, though at the expense of throughput. Furthermore, the spectrometer wavelength range is limited by the grating and detector and can thus be used at deep UV wavelengths. The AOTF and LCTF devices offer moderate spectral resolution relative to the imaging spectrometer, but much higher throughput.

Time-resolved plasma images can also be acquired by using recently developed tunable filter technologies along with an intensified charge-coupled detector (ICCD). Acousto-optic tunable filters (AOTF) and liquid crystal tunable filters (LCTF) operate on different principles, but they are both capable of rapid wavelength selection with microsecond to millisecond tuning speeds while preserving imaging integrity. Several articles have been published describing in detail the theory and principles on which AOTFs and LCTFs are based.<sup>32-39</sup> An AOTF is a diffraction based optical-band-pass filter that can be rapidly tuned to pass various wavelengths of light by varying the frequency of an acoustic wave propagating through an anisotropic crystal medium.<sup>33</sup> The LCTF is a birefringent filter, which uses the retardation, in phase, between the ordinary and extraordinary light rays passing through a liquid crystal to create constructive and destructive interference, to pass a single wavelength of light. By combining several electronically tunable stages in series, high spectral resolution can be achieved (e.g.,  $8 \text{ cm}^{-1}$ ).<sup>35</sup>

Tunable filters are most commonly used for Raman chemical imaging and fluorescence microscopy applica-

Received 1 November 2000; accepted 16 April 2001.

\* Author to whom correspondence should be sent.

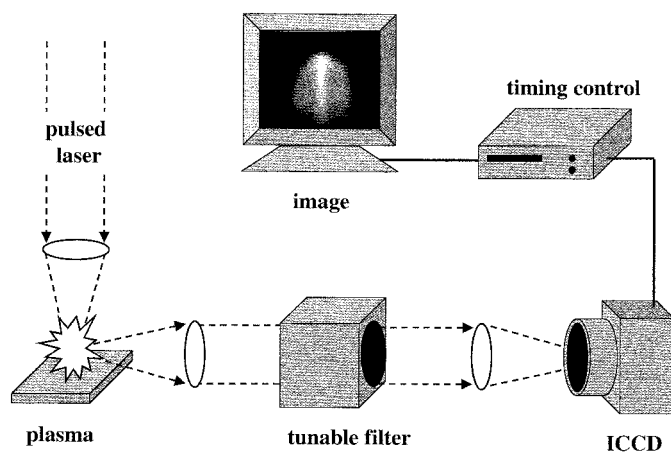


FIG. 1. Schematic diagram of the time-resolved plasma imaging setup consisting of either an acousto-optic or liquid crystal tunable filter along with an intensified charge coupled detector.

tions. Recent applications include Raman chemical imaging of breast tissue,<sup>40</sup> Raman chemical imaging of hazardous waste samples,<sup>41</sup> fluorescence detection of sub-cellular processes in living cells,<sup>35</sup> and fluorescence and Raman polymer characterization.<sup>39</sup> LIBS is unlike most other spectroscopic methods because of the intense broadband background caused by electron-ion collisions taking place within the plasma. The atomic and ionic emissions from the plasma span a wide range of wavelengths and consist of many lines. Unlike Raman spectroscopy, which is the primary technique for which tunable filters are used, the LIBS background is unpredictable and not easily rejected.

Time-resolved plasma imaging using AOTFs has been previously shown to be useful for investigating the spatial and temporal distribution of ionic and atomic lines,<sup>43</sup> the effect of the focusing lens,<sup>43,44</sup> the lens to sample distance,<sup>43,44</sup> the angle-of-incidence of the laser pulse onto the sample,<sup>43,44</sup> and the effect of atmospheric pressure on the size and shape of the resulting plasma.<sup>9</sup> In this paper, we report the first time-resolved plasma images acquired using a liquid crystal tunable filter. We also compare the use of AOTFs and LCTFs for time-resolved plasma imaging applications in terms of resolution, out-of-band rejection, and image quality.

## EXPERIMENTAL

The time-resolved plasma imaging setup used in this work is shown schematically in Fig. 1. To generate a laser-induced plasma, a Q-switched Nd:YAG laser (Continuum Surelite III) operated at 1064 nm and 80 mJ/pulse

was focused 1–2 mm beyond the surface of the sample by using an  $f/4$  lens. For all experiments described here, a laser repetition rate of 2 Hz was used.

The resulting plasma emission was collected and collimated via an  $f/4$  lens and passed through either the acousto-optic tunable filter (Brimrose Corporation of America, Model TEAF7–5.0–1.0–I) or the liquid crystal tunable filter (Cambridge Research & Instrumentation, Model V153). A comparison of various specifications and characteristics of the two tunable filter devices is tabulated in Table I.<sup>38,39</sup> The operating ranges of tunable filters are slightly different, with both devices having an operating range from 500 nm to 750 nm. Because of this, two target atomic lines that traverse the spectral range of the devices were chosen. Specifically, these were the 521.8 nm (copper (I)), and 722.9 nm (lead (I)) lines. Both devices are small, with high spectral resolution: typically 1–3 nm, and 0.25–0.5 nm for the AOTF and LCTF, respectively. Also, it is worth noting that both devices are capable of high spatial resolution ( $\sim 300$  nm) and the spatial resolution of these studies was limited by the pixel resolution of the ICCD camera being used and not the tunable filter devices.

The desired emission wavelengths were selected by the tunable filter and imaged by a gated ICCD (Princeton Instruments, Model ST-138 controller, Model PG-200 pulser, Model ITE/CCD-576-G/RE-E detector) equipped with a camera lens (Nikon, 35 mm). All plasma images were acquired 2.0  $\mu$ s after initial plasma formation. For laser-induced plasmas formed on steel samples, emission was collected using a 5  $\mu$ s gate width. All other experiments were conducted using a 0.5  $\mu$ s gate width. In addition, each plasma image represents the accumulated emission collected from 5 sequential plasmas after 30 pre-shots had been used to prepare the sample. Five replicate measurements were acquired at every wavelength selected, with a relative standard deviation of approximately 10%.

For spectral measurements, the output of the tunable filter was coupled to a 0.25 m,  $f/4$  spectrograph (Chromex Model 250IS/RF) via an optical fiber (Edmund Scientific Co. Model D2551). The detection system consisted of a gated ICCD similar to the one described above (Princeton Instruments, Model ITE/CCD-576-G/RB-E), with Model PG-200 pulser and Model ST-138 detector controller.

For spectral resolution calculations (Figs. 5 and 6), the full spectral width at half the maximum intensity (FWHM) of the spectral peaks were calculated from a Gaussian curve that was fit to the data.

TABLE I. Characteristics of the acousto-optic and liquid crystal tunable filters.

	AOTF <sup>a</sup>	LCTF <sup>b</sup>
Mode of operation	Solid state, Bragg diffraction	Solid state, interference
Dimensions	1.6 × 1.2 × 1.2 in.	3 × 3 × 3 in.
Aperture size	7 × 7 mm	20 mm radius
Tuning speed	250 $\mu$ s	50 ms
Spectral resolution	0.6–3.4 nm ( $\sim 20$ cm <sup>-1</sup> )	0.25–0.5 nm ( $\sim 8$ cm <sup>-1</sup> )
Miscellaneous	Image shift	No image shift

<sup>a</sup> Taken from Ref. 37.

<sup>b</sup> Taken from Ref. 38.

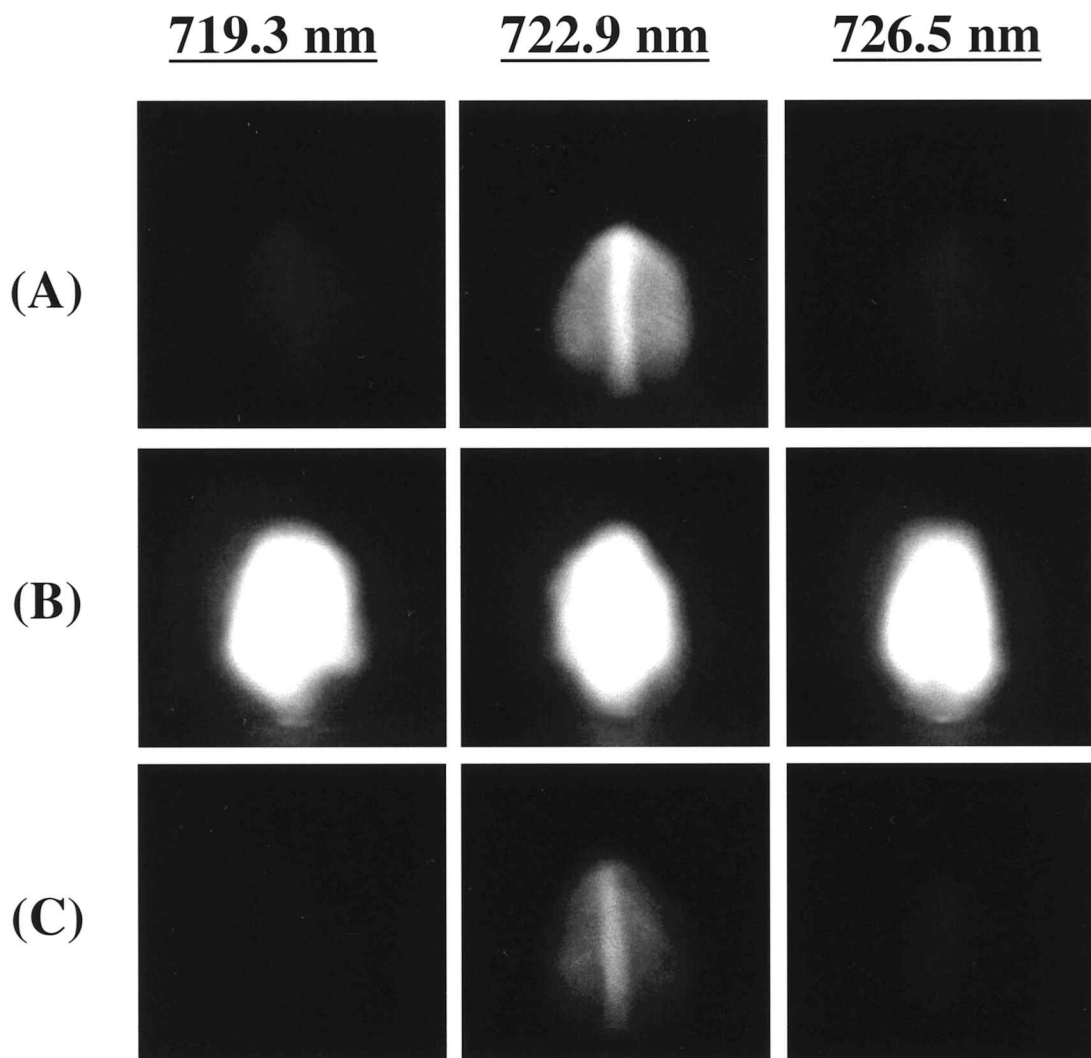


FIG. 2. Plasma images acquired on and off the 722.9 nm lead line 2.0  $\mu$ s after initial plasma formation by use of (A) an AOTF, (B) an LCTF, and (C) an LCTF and 750 nm short pass filter for wavelength selection.

## RESULTS AND DISCUSSION

Due to the inherent differences in principles of operation, acousto-optic (AOTF) and liquid crystal (LCTF) tunable filters possess slightly different characteristics, as shown in Table I.<sup>38,39</sup> Both devices are capable of rapid wavelength selection with microsecond tuning speeds while preserving imaging integrity. The differences in the devices which are of concern to plasma imaging addressed in this paper are out-of-band rejection, spectral resolution, and image quality.

Figure 2A shows images of a lead plasma taken with an AOTF. The images were all acquired 2  $\mu$ s after initial plasma formation, producing a plasma extending approximately 2–3 mm above the sample surface. The distribution of lead emission within the plasma (center image) was acquired by tuning the AOTF to an atomic lead line (722.9 nm). The 722.9 nm line was chosen because it is a strong emission line that is present within the tuning ranges of both filters. As found in previous lead plasma imaging studies, the distribution of lead emission within the plasma appears to be centrally located, with a column type shape.<sup>45</sup> Also shown in Fig. 2A, to either side of the lead plasma image, are images acquired by tuning the

AOTF to a spectral region where atomic emission was not observed, i.e., above (726.5 nm) and below (719.3 nm) the atomic line. In Fig. 2B, images acquired under the same experimental conditions, but with the LCTF, are shown. With the LCTF, a very high background was observed that masked the lead emission. The filtered emission was examined further by coupling the output of the LCTF (set to 722.9 nm) to a spectrometer. The spectral plot in Fig. 3A shows the 722.9 nm line passing through the LCTF along with an increased background in the 800 nm region and several other atomic lines at:  $\sim$ 777.2 nm, corresponding to oxygen emission, and 818.8 nm, 821.2 nm, and 826.1 nm, all corresponding to nitrogen emission. These lines lie outside the tuning range of the device (above 750 nm) and are minimally rejected by the LCTF. Hence, interference from O and N lines will always be a problem when imaging with an LCTF in an ambient atmosphere or any atmosphere containing large amounts of O<sub>2</sub> and N<sub>2</sub>. To overcome this problem, a 750 nm short pass filter was used when acquiring all remaining plasma images with the LCTF. Plasma images of the 722.9 nm lead line acquired using the LCTF and the 750 nm short pass (SP) filter are shown in Fig. 2C. It is clear

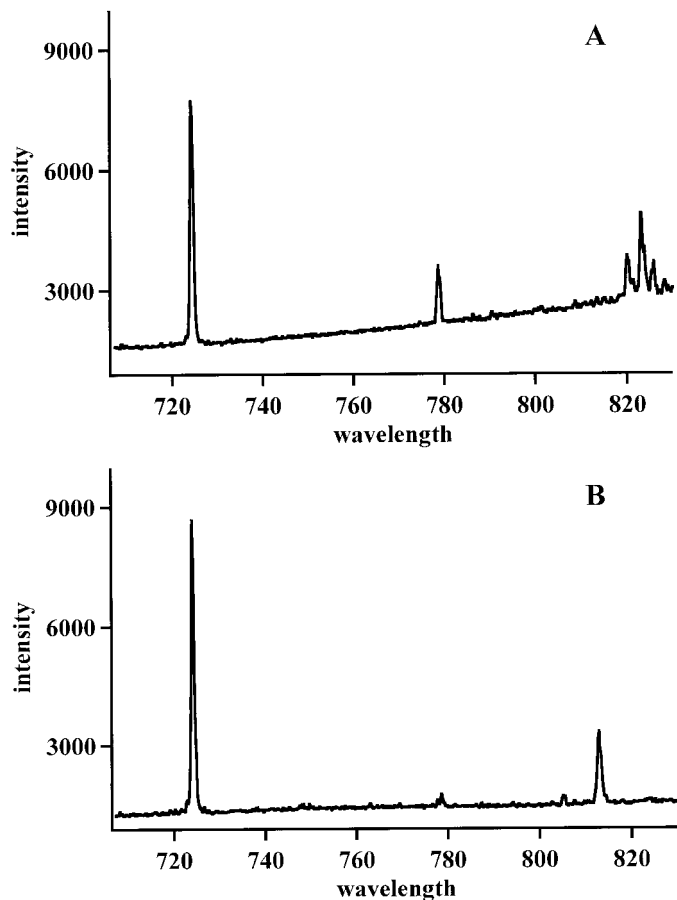


FIG. 3. The emission spectra of a LIBS plasma acquired with (A) the LCTF and (B) the AOTF coupled to a spectrometer, and with both devices set to the atomic lead line at 722.9 nm.

that use of the additional filter allows high quality images, comparable to those achieved with the AOTF (Fig. 2A), to be obtained.

Although not as much of a problem, there are instances, depending on the sample matrix, where very strong atomic or ionic lines can cause background problems when using the AOTF for wavelength selection. An example of this is shown in Fig. 3B, where the output of the AOTF, set to the 722.9 lead line, was coupled to a spectrograph. The line present at 811.4 nm is actually the second order of a very strong atomic lead line at 405.7 nm. This line lies below the tuning range of the AOTF ( $<500$  nm). Although the AOTF did reject most of this line intensity (roughly 98%), in cases where the atomic line is very strong, 2% out of band transmission could potentially cause significant background problems. This suggests that the use of an additional filter, such as a 500 nm long pass (LP), to reject wavelengths below the tuning range of the device may be required.

To examine the resolution of the two devices over the working range of the filters, both devices were scanned across a lead line in the upper working range of the filters (722.9 nm) and a copper line in the lower working range of the filters (521.8 nm). Figure 4 shows a selection of these images, which were acquired by scanning the filter wavelength with (A) the LCTF with a 750 nm SP filter and (B) the AOTF with a 500 nm LP filter across the 722.9 nm atomic lead line. The plasma emission of each image was integrated to create the spectra shown in Fig. 5. The LCTF scan (Fig. 5A) resulted in a narrower band-pass than that obtained using the AOTF (Fig. 5B). Specifically, the full width at half the maximum (FWHM) of the emission line was approximately 0.4 nm ( $8\text{ cm}^{-1}$ ) and 1.0 nm ( $19\text{ cm}^{-1}$ ) for the LCTF and AOTF, respectively. In the lower working range of the filters, the LCTF was also found to exhibit resolution superior to the AOTF. Figure 6 compares a scan across a 521.8 nm copper line

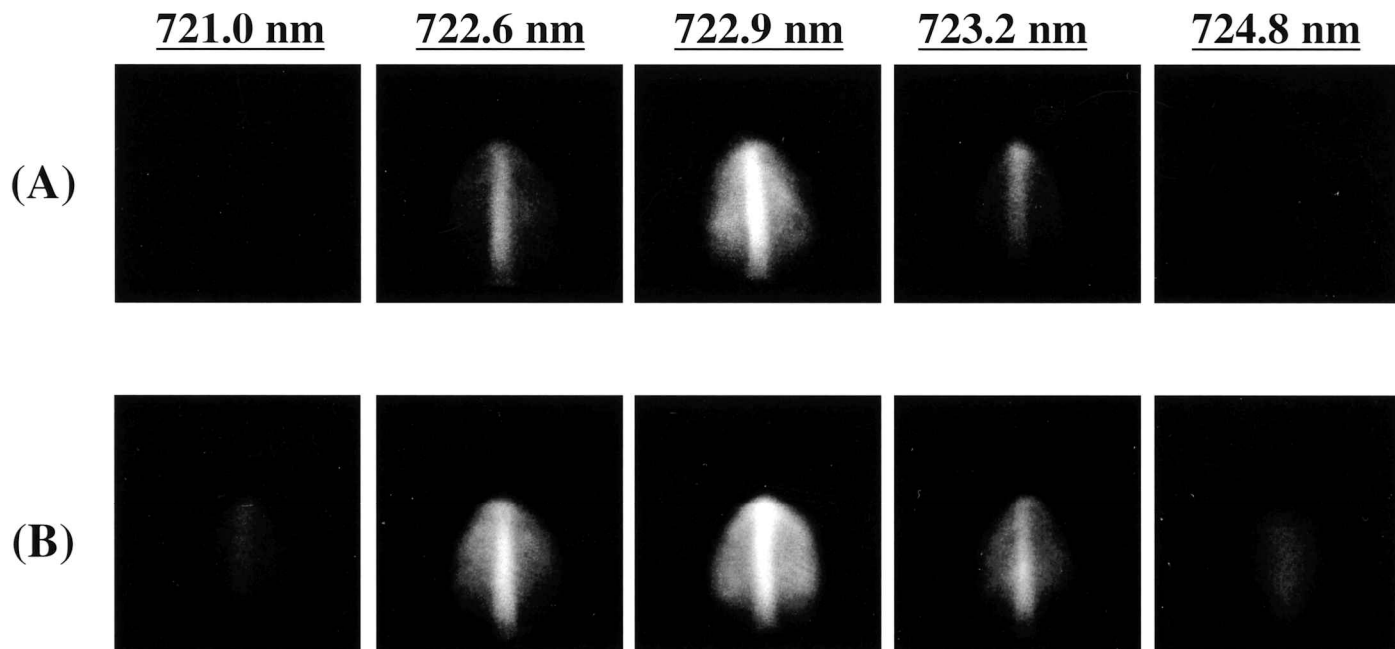


FIG. 4. Images of a laser-induced plasma generated on a lead sample acquired 2.0  $\mu\text{s}$  after initial plasma formation by scanning the wavelength of (A) the LCTF and (B) the AOTF.

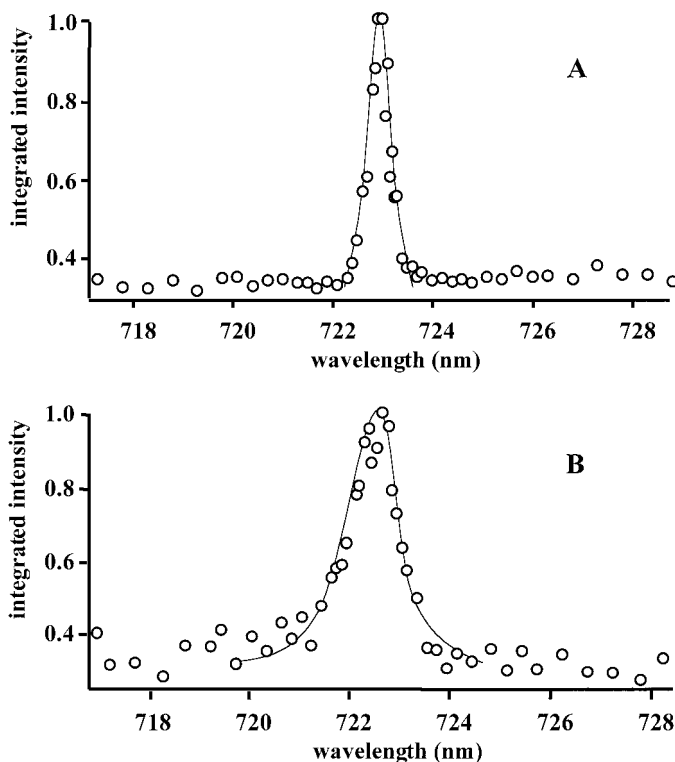


FIG. 5. Integrated emission intensity from lead plasma images acquired by scanning (A) the LCTF and (B) the AOTF wavelength across the 722.9 nm atomic lead line. All images were acquired 2.0  $\mu$ s after initial plasma formation.

obtained by using (A) the LCTF to one obtained with (B) the AOTF. The FWHM for this emission line was 0.25 nm ( $9\text{ cm}^{-1}$ ) for the LCTF and 0.6 nm ( $21\text{ cm}^{-1}$ ) using the AOTF. For both filters, the wavelength resolution tends to worsen with increasing wavelength. Not surprisingly, however, the resolution is fairly constant throughout the tuning range in terms of wavenumbers. This effect is not very important when conducting studies of pure samples with relatively few and well separated lines. However, when studying plasmas produced on complex samples with many emission lines, such as steel, high resolution is often needed. This is illustrated in Fig. 7, which compares the resulting atomic emission spectra of a steel sample obtained by integrating the emission intensity of each image from scans obtained by using (A) the LCTF and (B) the AOTF. From these spectra, it is apparent that the LCTF is capable of resolving the 522.7 nm and 523.3 nm iron lines, while the AOTF provides a poorly resolved spectrum. These results are typical for LIBS, but do not demonstrate the best that can be achieved with either device for other imaging applications. Furthermore, advances in the radio frequency driver and piezo-electric technologies associated with AOTFs have allowed for recent improvements, which includes a spectral bandpass ( $7.5\text{ cm}^{-1}$ ) comparable to the LCTF.<sup>46</sup>

## CONCLUSION

Because of the intense broadband background generated by laser-induced plasmas, imaging of atomic emission lines produced by these plasmas is unlike other spectroscopic imaging applications that rely on tunable fil-

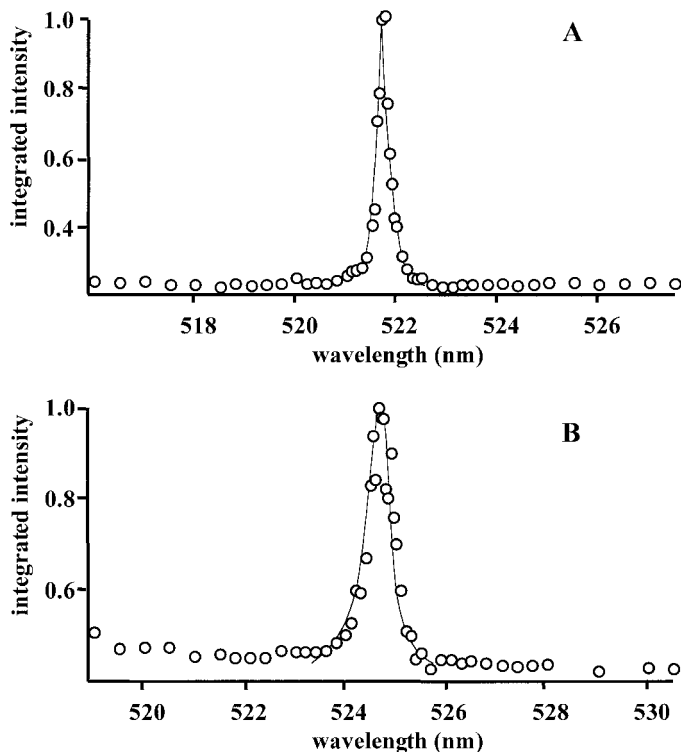


FIG. 6. Integrated emission intensity from copper plasma images acquired by scanning (A) the LCTF and (B) the AOTF wavelength across the 521.8 nm atomic copper line. All images were acquired 2.0  $\mu$ s after initial plasma formation.

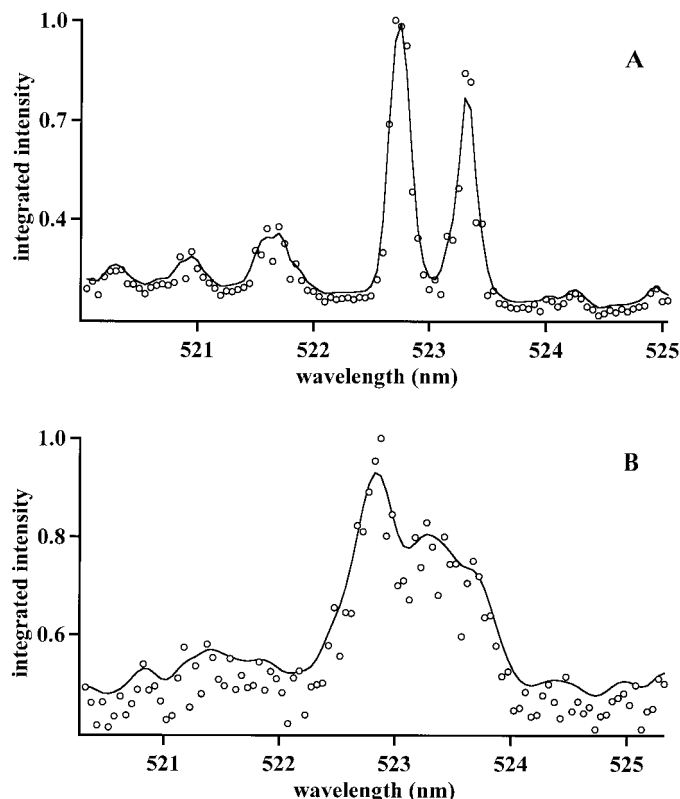


FIG. 7. Integrated emission intensity from plasma images produced on a steel sample, acquired by scanning (A) the LCTF and (B) the AOTF wavelength across iron lines from a steel sample. All images were acquired 2.0  $\mu$ s after initial plasma formation.

ters.<sup>35,39-41</sup> Despite this, high quality images of the distribution of atomic emission within a laser-induced plasma can be achieved by using both AOTFs and LCTFs. However, additional filters are needed for rejection of wavelengths out of the tuning range of the devices. Both devices exhibit the best resolution in the lower working wavelength range of the filters (~500 nm) and the LCTF exhibits superior spectral resolution overall.

#### ACKNOWLEDGMENTS

We would like to thank the U.S. Department of Energy for support of this work under Grant No. DEFG0796ER62305 and the Office of Naval Research for support of this work under Grant No. N0014-97-1-0806. We would also like to thank Dr. Mickey Myrick for the generous loan of an ICCD detection system.

1. D. A. Rusak, B. C. Castle, B. W. Smith, and J. D. Winefordner, *Crit. Rev. Anal. Chem.* **27**, 257 (1997).
2. K. Song, Y. I. Lee, and J. Sneddon, *Appl. Spectrosc. Rev.* **32**, 183 (1997).
3. J. Sneddon and Y. I. Lee, *Anal. Lett.* **32**, 2143 (1999).
4. D. A. Rusak, B. C. Castle, B. W. Smith, and J. D. Winefordner, *Trends Anal. Chem.* **17**, 453 (1998).
5. E. D. Lancaster, K. L. McNesby, R. G. Daniel, and A. W. Miziolek, *Appl. Opt.* **38**, 1476 (1999).
6. B. J. Marquardt, D. N. Stratis, D. A. Cremers, and S. M. Angel, *Appl. Spectrosc.* **52**, 1148 (1998).
7. B. J. Marquardt, S. R. Goode, and S. M. Angel, *Anal. Chem.* **68**, 977 (1996).
8. L. Burgio, R. J. H. Clark, T. Stratoudaki, M. Doulgeridis, and D. Anglos, *Appl. Spectrosc.* **54**, 463 (2000).
9. A. K. Knight, N. L. Scherbarth, D. A. Cremers, and M. J. Ferris, *Appl. Spectrosc.* **54**, 331 (2000).
10. D. Romero and J. J. Laserna, *Spectrochim. Acta, Part B* **55**, 1241 (2000).
11. R. Nyga and W. Neu, *Opt. Lett.* **18**, 747 (1993).
12. K. L. Eland, D. N. Stratis, J. C. Carter, and S. M. Angel, *Proc. SPIE - Int. Soc. Opt. Eng.* **3853**, 288 (1999).
13. P. Fichet, P. Mauchien, and C. Moulin, *Appl. Spectrosc.* **53**, 1111 (1999).
14. D. N. Stratis, K. L. Eland, and S. M. Angel, *Appl. Spectrosc.* **54**, 1719 (2000).
15. C. F. Su, S. M. Feng, J. P. Singh, F. Y. Yuen, J. T. Rigsby III, D. L. Monts, and R. L. Cook, *Glass Technol.* **41**, 16 (2000).
16. H. Lancelin, L. Dudragne, P. Adam, and J. Amouroux, *High Temp. Material Processes* **4**, 109 (2000).
17. L. J. Radziemski and D. A. Cremers, *Laser-Induced Plasmas and Applications*, L. J. Radziemski and D. A. Cremers, Eds. (Marcel Dekker, New York, 1989).
18. V. Bulatov, L. Xu, and I. Schechter, *Anal. Chem.* **68**, 2966 (1996).
19. B. C. Castle, K. Visser, B. W. Smith, and J. D. Winefordner, *Appl. Spectrosc.* **51**, 1017 (1997).
20. M. Tanaka, Y. Fujisawa, T. Nakajima, Y. Tasaka, K. Ota, and S. Usami, *J. Appl. Phys.* **83**, 3379 (1998).
21. B. C. Castle, K. Visser, B. W. Smith, and J. D. Winefordner, *Spectrochim. Acta, Part B* **52**, 1995 (1997).
22. Y. Iida, *Spectrochim. Acta, Part B* **45**, 1353 (1990).
23. G. Padmaja, A. V. R. Kumar, P. Radhakrishnan, V. P. N. Nampoori, and C. P. G. Vallabhan, *J. Phys. D: Appl. Phys.* **26**, 35 (1993).
24. S. S. Harilal, C. V. Bindhu, V. P. N. Nampoori, and C. P. G. Vallabhan, *Appl. Spectrosc.* **52**, 449 (1998).
25. G. Callies, P. Berger, and H. Hugel, *J. Phys. D: Appl. Phys.* **28**, 794 (1995).
26. H. Schittenhelm, G. Callies, P. Berger, and H. Hugel, *Appl. Surf. Sci.* **127-129**, 922 (1998).
27. J. D. Wu, Q. Pan, and S. C. Chen, *Appl. Spectrosc.* **51**, 883 (1997).
28. Y. Iida, *Spectrochim. Acta, Part B* **45**, 1353 (1990).
29. I. B. Gornushkin, M. Clara, B. W. Smith, J. D. Winefordner, U. Panne, and R. Niessner, *Spectrochim. Acta, Part B* **52**, 1617 (1997).
30. W. Whitty and J. P. Mosnier, *Appl. Surf. Sci.* **127-129**, 1035 (1998).
31. J. W. Olesik and G. M. Hieftje, *Anal. Chem.* **57**, 2049 (1985).
32. H. R. Morris, C. C. Hoyt, P. Miller, and P. J. Treado, *Appl. Spectrosc.* **50**, 805 (1996).
33. H. H. Morris, C. C. Hoyt, and P. J. Treado, *Appl. Spectrosc.* **48**, 857 (1994).
34. C. D. Tran, *Anal. Chem.* **64**, 971A (1992).
35. C. C. Hoyt and D. M. Benson, *Photonics Spectra* **26**, 92 (1992).
36. G. Fulton and G. Horlick, *Appl. Spectrosc.* **50**, 885 (1996).
37. D. P. Baldwin and D. S. Zamzow, *Talanta* **45**, 229 (1997).
38. AOTF Manual, model TEAF7-5.0-1.0-I, Brimrose Corporation of America, Baltimore, MD.
39. LCTF Manual, model V153, Chemicon Inc., Pittsburgh, PA.
40. N. J. Kline and P. J. Treado, *J. Raman Spectrosc.* **28**, 119 (1997).
41. J. R. Schoonover, F. Weesner, G. J. Havrilla, M. Sparrow, and P. Treado, *Appl. Spectrosc.* **52**, 1505 (1998).
42. H. R. Morris, B. Munroe, R. A. Ryntz, and P. J. Treado, *Langmuir* **14**, 2426 (1998).
43. R. A. Multari, L. E. Foster, D. A. Cremers, and M. J. Ferris, *Appl. Spectrosc.* **50**, 1483 (1996).
44. R. A. Multari and D. A. Cremers, *IEEE Transactions on Plasma Science* **24**, 39 (1996).
45. D. N. Stratis, K. L. Eland, and S. M. Angel, *Proc. SPIE - Int. Soc. Opt. Eng.* **3534**, 592 (1999).
46. B. M. Cullum, J. Mobley, Z. H. Chi, D. L. Stokes, G. H. Miller, and T. Vo-Dinh, *Rev. Sci. Instrum.* **71**, 1602 (2000).